JOURNAL OF MATERIALS SCIENCE 29 (1994) 2335–2340

R curves for energy dissipative materials

P. WILL
Department of Electrical Engineering, College for Technology and Economics, Technikumplatz 17, Mittweida D 09648, Germany

This paper focuses on the theoretical simulation of fracture and stable crack growth of specimens with non-local damage. The first law of thermodynamics allows the identification or definition of appropriate crack-driving forces. The results are compared with recent ideas on defining tearing resistance for uncontained yield through the energy dissipation rate. A hypothesis regarding the conversion of mechanical into thermal energies within the non-local damage region is formulated to model the fracture behaviour of energy dissipative materials with rising crack resistance characteristics. The material's capacity to develop non-local damage is assumed to decrease with the actual damage level. This decrease relates linearly with the remaining resources of the material in dissipating energy. The hypothesis, which proposes a square root function for theoretical *J–R* curves, is verified by the regression analysis of experimental data regarding a European round-robin test of different steels.

1. Introduction

This paper deals with the way in which the energy balance should be formulated when non-local damage processes associated with energy dissipation accompany crack growth. The question is raised whether fracture resistance relates to energy rate asssociated with material separation, or whether it is related to work consumed in fracture and non-local damage. The local energy balance is used to rearrange the relationships between the different energies consumed both in the process of material separation and due to non-local damaging (plastic deformation, microvoid growth and linkage, cracking of inclusions, transforming particles, stochastic fibre failure [1, 2]) around the crack tip. The energy balance aids the decision to utilize a measure of the total resistance to fracture or only the separation part as toughness.

2. Local energy balance

The total work done per unit time, $\delta\mathring{U}$, within a thin disc of thickness δx_3 (Fig. 1) can be related to the rate of change in the kinetic energy, $\delta\mathring{K}$, the recoverable internal energy rate, $\delta\mathring{W}$, and the energy, $\delta\mathring{\Phi}$, consumed irreversibly per unit time in an energy dissipative damage region, A_0, by

$$\delta\mathring{U} = \delta\mathring{K} + \delta\mathring{W} + \delta\mathring{\Phi} \tag{1}$$

$\delta\mathring{\Phi}$ includes the energy used up just in material separation. The symbol δ points explicitly to the peculiarities in considering an infinitesimally thin disc, which has been chosen to obtain a model for local fracture behaviour. The total energy rate is the sum of mechanical and thermal work done per unit time within the volume δV (first integral) and through its surface (A-top + A-bottom + $\Gamma\delta x_3$). The region A excludes the damage region A_0 shielding the crack tip.

$$\delta\mathring{U} = \delta x_3 \left[\int_A \int (F_i \mathring{u}_i + h)\mathrm{d}A + \int_A \int (\mathring{u}_i \sigma_{i3} - q_3)_3 \mathrm{d}A + \int_\Gamma (\mathring{u}_i \sigma_{ik} - q_k) n_k \mathrm{d}\Gamma \right] \tag{2}$$

where F = body force; $\mathring{u}$ = displacement velocity h = heat sources; σ_{ik} = components of the (first Piola–Kirchhoff) stress tensor; q = heat flux; and $\boldsymbol{n}$ = outer unit normal vector (two-dimensional). A dot marks total time derivative, indices following a comma denote local, partial derivatives. The local derivative in the second integral is based on the different signs of the unit vectors associated with A-top and A-bottom.

$$\delta\mathring{K} + \delta\mathring{W} = \delta x_3 \int_A \int \rho(\mathring{k} + \mathring{w})\mathrm{d}A - \iint_{\delta A_0(t)} \rho(k + w) v_j n_j^{\mathrm{A}} \mathrm{d}A \tag{3}$$

The symbols k and w denote the specific kinetic and internal energy density, respectively. The second integral accounts for the momentary change of the orientable interface $\delta A_0(t)$ between the damage region and its surrounding. Usually, the time dependence of the integration boundary $\delta A_0(t)$ has been neglected. Each single component of $\delta A_0(t)$ moves with a corresponding local velocity, v, taking into account a potential growth of the damage region. Generally, the interface is curved. Its local unit normal vector $\boldsymbol{n}^{\mathrm{A}}$ is a three-dimensional one in contradiction to $\boldsymbol{n}$, which is within the (1, 2)-plane only. The minus sign of the second term originates from the definition of $\boldsymbol{n}^{\mathrm{A}}$, which points to the surrounding region A. The local energy

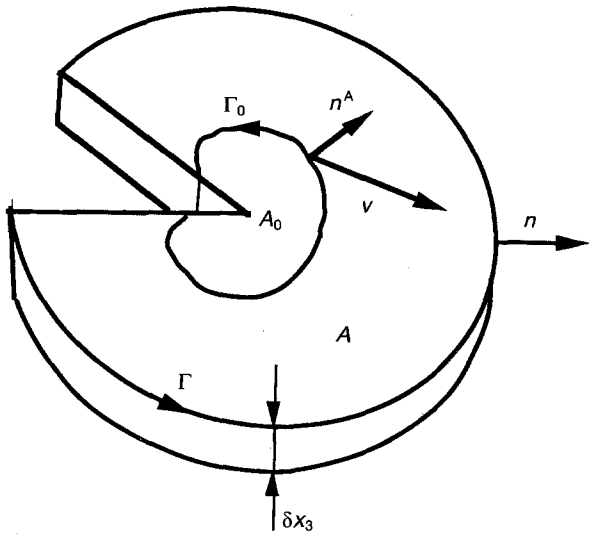

Figure 1 Local crack front with energy dissipative damage region, A_0.

change rate balance, which is valid only in the region beyond A_0 is given by:

$$\rho\mathring{w} = \sigma_{ij}\mathring{u}_{i,j} - q_{i,i} + h \tag{4}$$

In order to simplify the integrals in Equations 2 and 3, the divergence theorem of Gauss is invoked to replace the surface integrals regarding heat flux by a volume integral:

$$\delta x_3\left[\int_\Gamma q_k n_k \mathrm{d}\Gamma + \int_A\int q_{3,3}\mathrm{d}A\right] - \iint_{\delta A_0(t)} q_k n_k^A \mathrm{d}A = \delta x_3 \int_A\int q_{k,k}\mathrm{d}A \tag{5}$$

Note that Equation 5 is a special way of writing the divergence theorem, taking into account the peculiarities of an infinitesimally thin disc. $\delta x_3 A$ is the volume enclosed by A-bottom, A-top, the external boundary $\delta x_3\Gamma$ and the internal surface $\delta A_0(t)$. The second term corresponds to two surface integrals. The partial x_3-derivative originates from the different signs of the outer unit normal vectors characterizing A-top and A-bottom. Combining Equations 1–5 gives

$$\lim_{\delta x_3 \to 0}\frac{\delta\mathring{\Phi}}{\delta x_3} \equiv \mathring{\Pi} = \int_\Gamma (\mathring{u}_i\sigma_{ik}n_k)\mathrm{d}\Gamma - \int_A\int(\rho\mathring{u}_i\ddot{\mathring{u}}_i - F_i\mathring{u}_i + \sigma_{ij}\mathring{u}_{i,j})\mathrm{d}A + \int_A\int(\mathring{u}_i\sigma_{i3})_{,3}\mathrm{d}A + \int_{\Gamma_0(t)}\rho(k+w)(v_jn_j+v_3)\mathrm{d}\Gamma - \int_{\Gamma_0(t)}(q_jn_j+q_3)\mathrm{d}\Gamma \tag{6}$$

Equation 6 corresponds to a change from the global energy balance of the volume δV to a local energy balance in the plane x_3 = constant. $\boldsymbol{n}$ denotes the plane unit normal vector to Γ_0. The relationships between the three components of the unit normal vector $\boldsymbol{n}^A$ to the curved interface δA_0 and the two components of $\boldsymbol{n}$ are given by [3]

$$n_i = \frac{n_i^A}{(1-n_3^{A^2})^{1/2}} \quad (j = 1,2) \tag{7}$$

Assuming stable crack advance the actual crack length, a, correlates straightforwardly with time. Changing from the space-fixed coordinate system to a moving reference system, which is attached on the crack tip or strictly speaking on the centre of the damage region, and excluding explicit time-dependent dynamic loading gives

$$\mathring{u}_i = -u_{i,j}\mathring{a}_j \tag{8}$$

The velocity $\mathring{a}$ characterizes the crack growth rate. Now Equation 6 is modified to

$$\mathring{\Pi} = \Big[-\int_\Gamma u_{i,k}\sigma_{ij}n_j\mathrm{d}\Gamma + \int_A\int(\rho k_{,k} - F_iu_{i,k} + \sigma_{ij}u_{i,jk})\mathrm{d}A + \int_A\int(u_{i,k}\sigma_{i3})_{,3}\mathrm{d}A + \int_{\Gamma_0}\rho(k+w)(n_k+\delta_{k3})\mathrm{d}\Gamma\Big]\mathring{a}_k - \int_{\Gamma_0}\rho(k+w)(n_k+\delta_{k3})\Delta v_k\mathrm{d}\Gamma + \int_{\Gamma_0}(q_jn_j+q_3)\mathrm{d}\Gamma \tag{9}$$

with

$$\Delta v = v - \mathring{a} \tag{10}$$

The terms in brackets may be interpreted as the real crack driving force, because they are the only ones which associate directly with crack advance. The meaning of the bracketed expression in Equation 9 corresponds to that of the elastic energy release rate per unit thickness for real elastic–plastic materials, I, defined by Turner [4] some years ago. But generalizing Turner's fracture parameter, I, the expressions summarized by the brackets denote the components of a vector $\boldsymbol{J}^*$. To avoid confusion with the I-integral of Aoki *et al.* [5], the symbol $\boldsymbol{J}^*$ has been chosen to mark the crack driving force.

The concept of a damage region around the crack has been ill-defined hitherto. Therefore a critical internal energy density, ρw_0, specific to the material, is brought in which defines the outer contour, Γ_0, of the damage region with the cross sectional area, A_0. Neglecting kinetic energies and assuming $\rho w = \rho w_0$ on Γ_0 gives

$$\rho w_0\int_{\Gamma_0}(n_k+\delta_{k3})\mathrm{d}\Gamma = 0 \tag{11}$$

which means that the last integral in the brackets vanishes, and

$$\rho w_0\int_{\Gamma_0}(n_k+\delta_{k3})\Delta v_k\mathrm{d}\Gamma = \rho w_0\frac{\mathrm{d}A_0}{\mathrm{d}t}. \tag{12}$$

As long as the non-local damage zone is embedded within a non-damaged 'singularity' region (contained yielding) the J^* integrals are 'path independent', provided the outer contour Γ is beyond the inner boundary Γ_0. Their values are then always

$$J_k^* = -\int_{\Gamma_0} u_{i,k}\sigma_{ij}n_j d\Gamma \quad (k = 1,2,3) \qquad (13)$$

If the contour Γ_0 approaches the specimen boundaries (uncontained yielding) both the crack driving force, J^*, and the fracture energy rate, $\mathring{\Pi}$, become system-dependent.

The first law of thermodynamics, depicted mathematically by Equation 9, gives the motivation to apply J^* as a crack-driving force. It does not allow any statement on its critical values which control crack growth initiation or stable crack advance. Only additional assumptions [6] accounting for energy dissipation yield an appropriate criterion for stable crack growth. In order to discuss the conversion of mechanical into thermal energies, the energy balance Equation 9 may be simplified invoking Equations 12 and 13

$$d\Pi = J_k^* da_k + \rho w_0 dA_0 - \langle T\rangle dS \qquad (14)$$

where $\langle T\rangle$ = medium temperature of the non-local damage region, and S = entropy.

3. Stable crack growth

The schematic depiction (Equation 14) of energy balance Equation 9 justifies a differentiation between energies used for crack driving and work dissipated in non-local damaging. Commonly, fracture tests do not capture the energy dissipated in heat. The first two terms of Equation 14 correspond to an increment of the 'available energy dissipation', introduced by Turner [7], taking into consideration that the dominant term in real elastic–plastic material fracture tests is the work rate used up by the combined plastic deformation and the fracture process. The third term denotes the heat transfer through the boundary Γ_0 of the non-local damage region at temperature $\langle T\rangle$. Comparing the original energy balance (Equation 1), Equation 14 and the definition of Turner's energy dissipation rate, D, gives

$$D = \frac{d(\bar{U} - \bar{W})}{Bda} = \frac{1}{B}\int_0^B \left[J^* + \rho w_0 \frac{dA_0}{da}\right] dx_3 \qquad (15)$$

The right-hand side of Equation 15 describes the total crack-growth resistance. The left-hand side may be seen as the crack-driving force. Note that the change, $d\bar{W}$, in internal energy averaged over thickness, B, excludes heat flux. This means it accounts only for the elastic strain energy (Equation 4).

Equation 15 says that the crack-growth resistance and the crack-driving force must have the same size. It provides a condition for crack extension which is only necessary but not sufficient. An additional assumption is needed to characterize stable crack growth. The term describing the growth of the non-local damage region is not available to the actual separation process. Therefore it should be more appropriate to use a crack-growth resistance curve based immediately on the J^* integral as the fracture energy rate. Much of the work input is dissipated in plasticity which damages material adjacent to the crack but may not contribute directly to the crack driving force J^*. Neglecting residual stresses, this means

$$\rho w_0 \frac{dA_0}{da} = \langle T\rangle \frac{dS}{da} \qquad (16)$$

and therefore

$$\frac{d\Pi}{da} = J^* \qquad (17)$$

Accounting for conversion of mechanical into thermal energies, which is done by Equation 16, Equation 17 characterizes the mechanical energy consumed in stable material separation. The crack extension force has to be determined from the energy change arising from crack advance in the presence of the shielding process region, but without producing new plasticity or non-local damage. Fracture toughening originates from the reduced crack-driving force by internal shielding. Following the notation of Turner [4], the elastic energy release rate for real elastic–plastic material has been defined as I, with the remark that the physical meaning of I as the elastic energy release rate for real elastic–plastic material corresponds with that of the present author's J^*. But a significant difference between J^* and I arises out of averaging the latter over the thickness, B.

4. Laboratory measurement

Assuming contained yield, the energy release rate interpretation of J^* corresponds approximately with the laboratory measurement, J_D, based on a deformation plasticity assumption [8] for elastic–plastic material behaviour. Both J^* and J_D exclude the energy dissipated in producing new non-local damage or plasticity. Generally, both the crack length and the size of the non-local damage region vary under a J–R curve test. Invoking the deformation theory of plasticity, the actual loading path of the load–displacement curve $P(\Delta)$ is substituted by a deformation path (Fig. 2) representing the load–displacement behaviour when the crack size is fixed. The area under this curve represents the strain energy in a non-linear elastic material. The laboratory evaluation of J_D is based on the fictitious non-linear elastic loading curve. When the J integral for an elastic–plastic material is determined by this method, the energy release rate interpretation of J is restored. A significant difference between J^* and J_D originates from the definition of the former as a local fracture parameter characterizing the crack growth behaviour in the cross sectional area (x_3 = constant) in contradiction to the 'global' measurement J_D averaged over the thickness, B, or net thickness as appropriate. Utilizing single-specimen unloading compliance tests the actual values of J_D are calculated incrementally, as the deformation path depends on crack length. Only the components Δ_i and

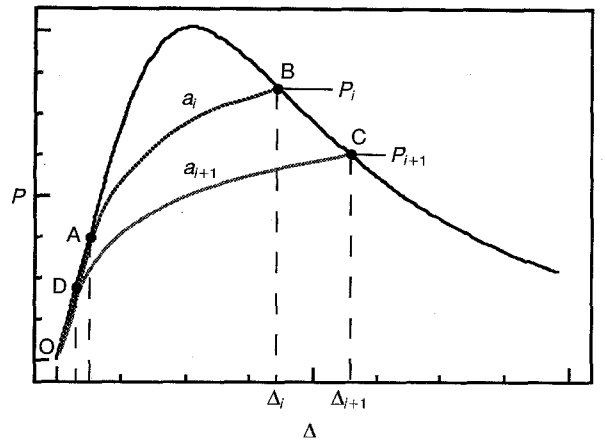

Figure 2 Schematic load–displacement curve for a specimen with a crack growing to a_{i+1} and a_i. The curves OB and OC represent the deformation paths associated with the two crack lengths a_i and a_{i+1}, respectively.

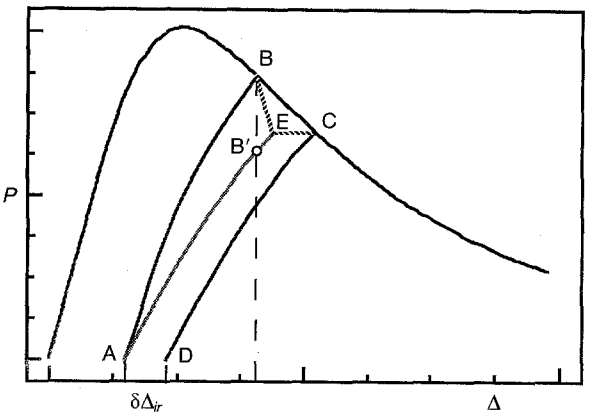

Figure 3 Cyclic load-unloading test.

Δ_{i+1}, which show a non-linear behaviour between AB and DC, respectively, need be considered here. The corresponding linear elastic terms can be determined from the current load and crack size.

$$J_{i+1} \approx \left[J_i + \left(\frac{\eta_{i+1}}{B b_{i+1}} \right) \frac{(P_{i+1} + P_i)(\Delta_{i+1} - \Delta_i)}{2} \right] \times \left[1 - \gamma_i \frac{a_{i+1} - a_i}{b_i} \right] \quad (18)$$

where $\eta = 2$, $\gamma = 1$ (SENB specimen); and $\eta = 2 + 0.522\, b/W$, $\gamma \approx 1 + 0.76\, b/W$ (CT specimen).

If the steps of crack growth are small, the actual deformation path need not be known precisely for a good estimate of J.

In order to carry out an experiment in accordance with the theoretical results of section 3, a cyclic load–unloading test with crack growth may be used, as proposed by Sakai [9]. As shown in Fig. 3, the curved loading path DC of a loading-unloading cycle is shifted to the loading path AB of the foregoing cycle by the irreversible residual part $\delta\Delta_{ir}$ of the displacement. Then the curved triangle ABE is constructed. The contours AB and AE correspond to the load–displacement relations for two specimens with different crack lengths a and $a + \delta a$, respectively. The enclosed area, δU, which accounts for crack-tip shielding, is seen to be approximately equivalent to

$$\delta U = J^* B \delta a \quad (19)$$

The region AECD is equivalent to $B\rho w_0 \delta A_0$. It is consumed to non-local damage.

5. Regression analysis

If the stress field near the crack tip is dominated by J^*, provided that J^* control exists, which implies that the stress field still scales with $J^*/\sigma_0 r$, the left-hand side of Equation 16 correlates in a straightforward relationship [3, 8] with the derivation of J^{*2}

$$\rho w_0 \frac{dA_0}{da} \propto J^* \frac{dJ^*}{da} \quad (20)$$

Chow & Lu [10] deduced an analogous expression for non-local damaged, softened materials. According to Steven & Guiu [11], the relation above means that the energy dissipating process has its effect on fracture, because it alters the stress state around the crack tip (shielding) and thus reduces the crack driving force J^* for crack growth. The work done by non-local damaging does not increase the resistance against separation of material. Equation 20 becomes invalid as specimen boundaries interact with the damage region.

Reanalysing data of Mecklenburg & Joyce [12], Turner has found that the energy rate consumed during fracture decreases nonlinearly with stable crack extension, approaching a constant value. Braga [13] reports on analogous behaviour for a 6-2-1-1 titanium alloy. Finally, the energy rate consumed in the damage region of tough ceramics has been experimentally observed [14] to diminish rapidly with stable crack extension. In the latter case, the micromechanical toughening processes like crack bridging work only in a small crack-opening regime.

As a working hypothesis [15] the author assumes that these decreases relate linearly with the remaining resources of the material in dissipating that energy which would be available to accelerate crack growth. Assuming J^*-controlled crack advance, it is specified mathematically by

$$\rho w_0 \frac{dA_0}{da} = T \frac{dS}{da} \propto \frac{J_c^2 - J^{*2}}{2r^*} \quad (21)$$

The energy rate consumed by non-local damaging beyond blunting is assumed to be specific of the material and to vary with the actual crack driving force J^* or damage level. Equation 21, characterizing the condition for stable crack growth, implies a rising crack resistance curve. The integration of this parametric equation results in

$$J_R = \left[J_c^2 - (J_c^2 - J_I^2) \exp\left(\frac{-\Delta a}{r^*} \right) \right]^{1/2} \quad J_R > J_I \quad (22)$$

The value of the parameter r^* is seen to correspond to the maximum possible non-local damage zone size that the material can accumulate. Possibly, specimen size values are so far below the material's capacity to develop non-local damage corresponding to r^* that

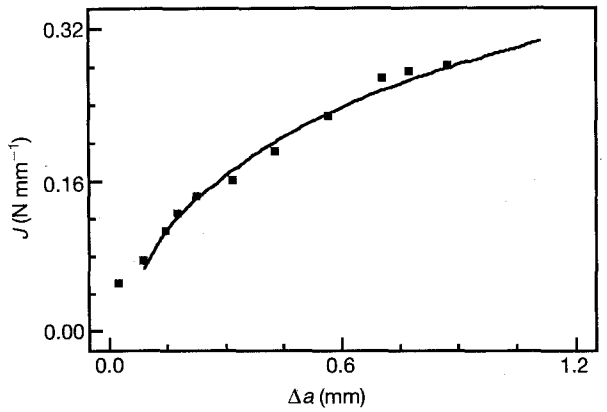

Figure 4 J–R curve (Si_3N_4) SENB at 1200 °C.

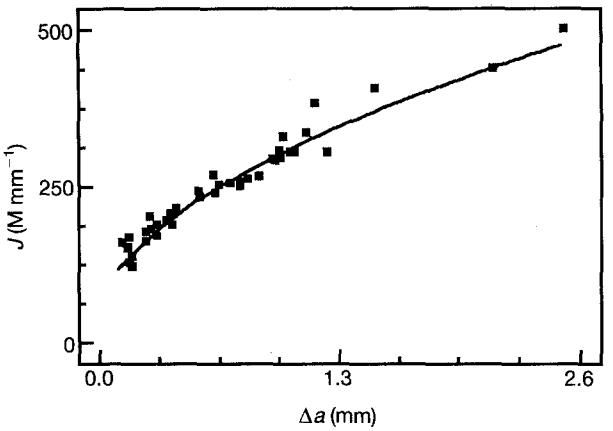

Figure 6 J–R curve (BS 4360-50E) medium-toughness material, CT-specimen.

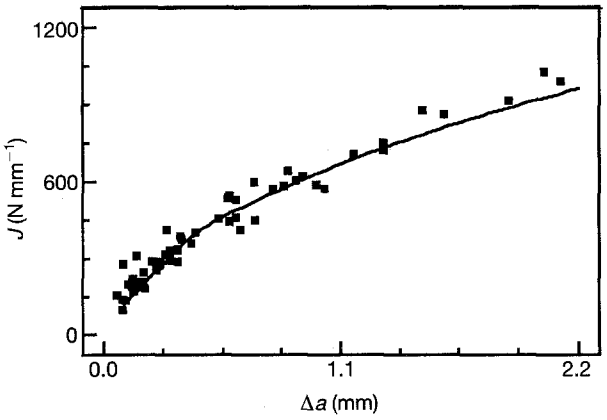

Figure 5 J–R curve (BS 1501-224-LT50) high-toughness material, CT-specimen.

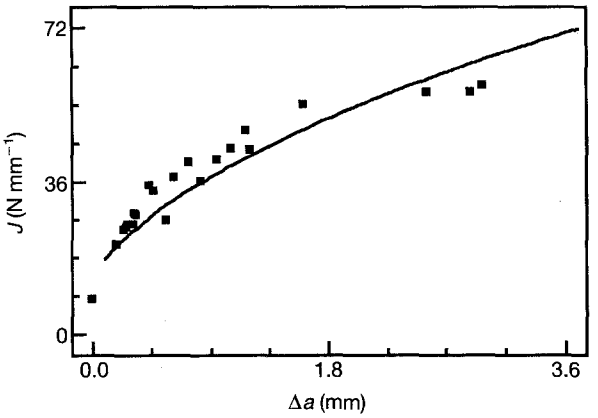

Figure 7 J–R curve (5083-0) low-toughness material, CT-specimen.

TABLE I J–R curve regression analysis $(A + C_R\Delta a)^{1/2}$

Toughness specimen	$A(N^2/mm^2)$	$C_R(N^2/mm^3)$	C_D (%)	ΔJ (N/mm)
High CT	-30690 ± 9400	432900 ± 29000	94	48
High SENB	-30000 ± 13500	476400 ± 36800	95	51
Medium CT	4826 ± 3700	88240 ± 6500	95	18
Medium SENB	4242 ± 3600	95160 ± 7300	96	16
Low CT	176 ± 120	1339 ± 200	91	5
Low SENB	47 ± 120	1943 ± 200	94	3

Confidence level 95%.
C_D = coefficient of determination; ΔJ = standard deviation.

the specimen size acts as a limiting factor (uncontained yielding). Note that then Equation 21 becomes questionable. The fracture resistance J_R itself is seen as a macroscopic instability value associated with a critical damage in the micro scale. The integration parameter J_I is the threshold where a critical level of initial non-local damage has been reached and fracture ensues. Equation 22 characterizes the real fracture behaviour only beyond an apparent, system-dependent crack advance $a_I - a_0$, because single specimen unloading compliance tests may reflect the initial non-local damage as real crack growth.

6. Discussion

Equation 21, like any other fracture criterion, can only be verified by comparison with experimental data. The result of a regression analysis [16] is shown in Fig. 4, where experimental data for a Si_3N_4–ceramic at 1200 °C from the cyclic loading–unloading test, corresponding to Fig. 3 and the theoretical J_R curve (Equation 22) are plotted together. This emphasizes Equation 21 which was proposed to explain the fracture behaviour of non-local damaged materials with rising crack resistance characteristics.

Assuming small crack advance in comparison with the maximum damage zone size parameter, r^*, the exponential function in Equation 22 may be approached by a series expansion. Neglecting the higher order terms gives

$$J_R \approx \left[J_I^2 + (J_c^2 - J_I^2)\frac{a - a_I}{r^*} \right]^{1/2} = (A + C_R\Delta a)^{1/2} \qquad r^* > a > a_I \quad (23)$$

The parameter C_R characterizes the initial resources of the material to convert mechanical into thermal

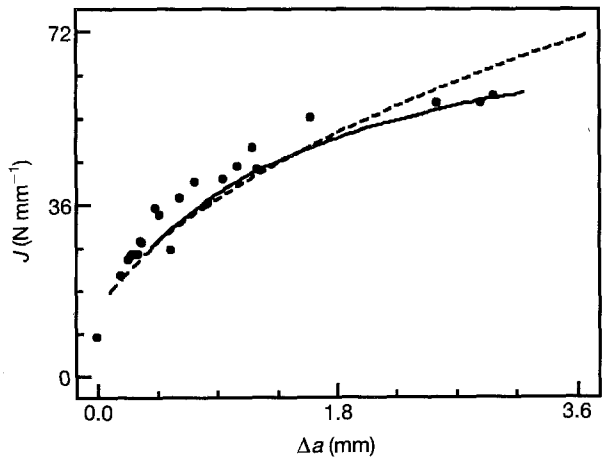

Figure 8 Comparison of J–R curves (low-toughness material). Equation 22, (——); Equation 23, (------).

energies. The regression analysis (Table I) of experimental data (Figs 5–7) regarding a European round-robin test of different steels [17] confirms the square root function (Equation 23) for a theoretical J–R curve.

These results confirm Equation 21. Note that the range of crack advance, which is represented in Fig. 7 for the low toughness material, seems to exceed the non-local damage zone size parameter r^* and the regression function (Equaion 23) becomes unusable, and should be replaced by Equation 22, as shown in Fig. 8.

Acknowledgements

The author would like to thank Professor Dr C. E. Turner, Dr B. Curr and Mr C. Noad for their hospitality and helpful discussions regarding the above results during a visit to Imperial College.

References

1. V. TVERGAARD and A. NEEDLEMAN, *Acta Metall.* **32** (1984) 157.
2. P. J. BUDDEN, and M. R. JONES, *Fatigue Fract. Engng. Mater. Struct.* **14** (1991) 469.
3. P. WILL, *Fortschrittberichte VDI Reihe* **18** (1988) 56.
4. C. E. TURNER, in: "Post-yield Fracture Mechanics", edited by D. G. H. Latzko, C. E. Turner, J. D. Landes, D. E. McCabe and T. K. Hellen, (Elsevier, Barking, 1984) p. 25.
5. S. AOKI, K. KISHIMOTO, M. SAKATA, *J. Appl. Mech.* **48** (1981) 825.
6. O. KOLEDNIK, *ESIS Newsletter* No. 20 (1992/93) 12.
7. C. E. TURNER, *ESIS Newsletter* No. 19 (1992) 10.
8. T. L. ANDERSON, "Fracture Mechanics" (CRC Press, Boca Raton, 1991).
9. M. SAKAI, J. I. YOSHIMURA, Y. GOTO, M. INAGAKI, *J. Amer. Ceram. Soc.* **71** (1988) 609.
10. C. L. CHOW and T. J. LU, *Int. J. Fract.* **50** (1991) 79.
11. R. N. STEVENS, F. GUIU, *Proc. R. Soc. Lond.* **A435** (1991) 169.
12. M. F. MECKLENBURG, J. A. JOYCE, P. ALBRECHT, in "Nonlinear fracture mechanics" Vol. II, "Elastic-plastic fracture", edited by J. D. Landes, A. Saxena and J. G. Merkle (ASTM STP 995, 1989) 594.
13. M. L. BRAGA, PhD thesis, Faculty of Engineering, Imperial College, University of London, 1992.
14. D. B. MARSHALL, M. V. SWAIN, *J. Amer. Ceram. Soc.* **71** (1988) 399.
15. P. WILL, B. MICHEL, P. KUNTZSCH, *cfiBer./DKG* **70** (1993) 23.
16. P. WILL, *Fortschrittsberichte der DKG* **3** (1992) 133.
17. B. HAYES, *et al.* Final report of a European round-robin, TWI Report No. 8029/6/90, The Welding Institute, Abington, 1990.

Received 29 April
and accepted 6 October 1993